H. C. Manoharan, C. P. Lutz, D. M. Eigler, Quantum mirages formed by coherent projection of electronic structure, *Nature*, **403** (2000) 512.

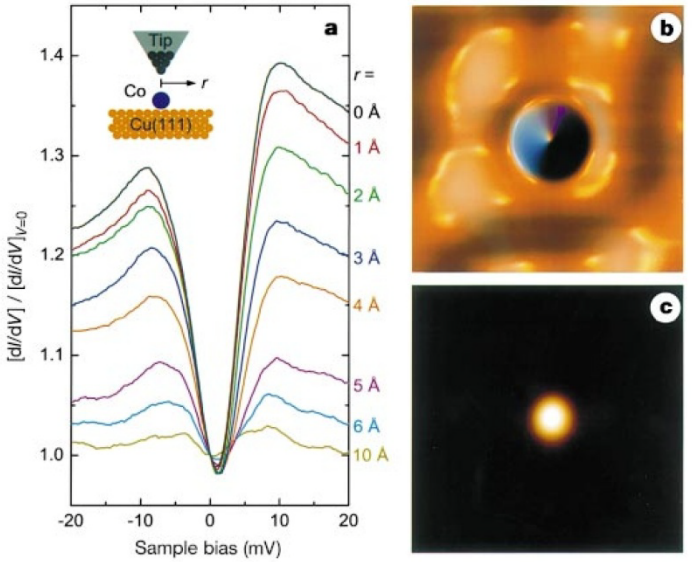

Figure 1 Detection of the Kondo resonance localized around a single Co atom on Cu(111). **a**, Tunnel spectra (normalized d*I*/d*V*) acquired over the Co atom for increasing lateral displacement *r* ($R_T = 100\,M\Omega$ at $V = 10\,mV$). Inset, measurement geometry. **b**, 35-Å square topograph ($V = 5\,mV$, $I = 1\,nA$) of an isolated Co atom (0.8-Å-high central bump) **c**, d*I*/d*V* map of the same area (average of $V = \pm 5\,mV$ acquisitions, $V_{a.c.} = 1\,mV$ r.m.s., $I = 1\,nA$). Dark to light corresponds to increasing conductance. Examples of the three types of data obtained in this experiment: (1) Topograph images (**b**) were acquired with the scanning tunnelling microscope (STM) operating in constant d.c. current (*I*) mode, in which a closed feedback loop constantly adjusted tip height. (2) Tunnel spectra (**a**) were acquired by adding a small a.c. modulation $V_{a.c.}$ (1 mV r.m.s. at 201 Hz) to the d.c. bias *V*, opening the feedback loop (hence, holding the tip motionless with respect to the surface), and measuring d*I*/d*V* versus *V* through lock-in detection of the a.c. component of the tunnel current. Such spectra were essentially independent of the tunnel junction impedance R_T, determined by *V*/*I* before opening the feedback loop. (3) d*I*/d*V* image maps (**c**) were acquired simultaneously with associated topographs by applying an a.c. modulation (typically 250 μV to 1 mV r.m.s. at 201 or 1007 Hz) at a frequency exceeding the bandwidth of the feedback loop, and recording the lock-in detected d*I*/d*V* (conductance map) along with tip height (topograph) at fixed d.c. bias *V* while the tip was scanned in closed-loop constant-*I* mode. Both kinds of differential conductance measurements constitute a probe of the local density of states under the tip[17,18].

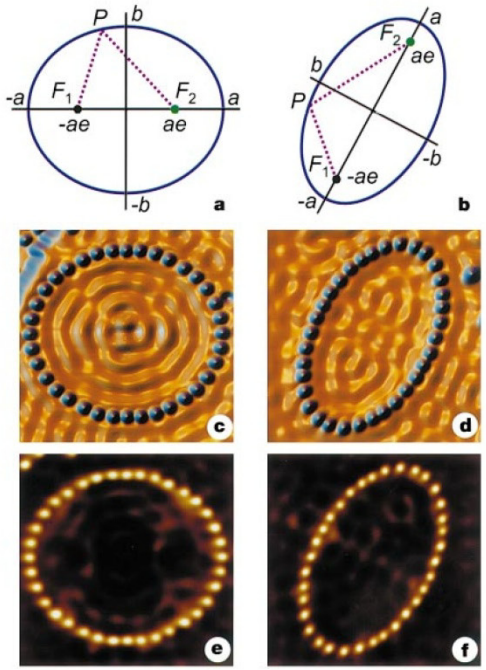

Figure 2 Elliptical electron resonators. **a**, Eccentricity $e = 1/2$; **b**, $e = 0.786$. **c**, **d**, Corresponding topographs of the experimental realizations ($a = 71.3$ Å for both ellipses) employing Co atoms to corral two-dimensional electrons on Cu(111). **e**, **f**, d*I*/d*V* maps acquired simultaneously with the corresponding topographs, tuned to image the Kondo resonance. ($V = 10$ mV, $V_{a.c.} = 250$ μV r.m.s., $I = 1$ nA for **c** and **e**; $V = 8$ mV, $V_{a.c.} = 1$ mV r.m.s., $I = 1$ nA for **d** and **f**). Image dimensions are 150 Å square and 154 Å square for the $e = 1/2$ and $e = 0.786$ ellipses, respectively.

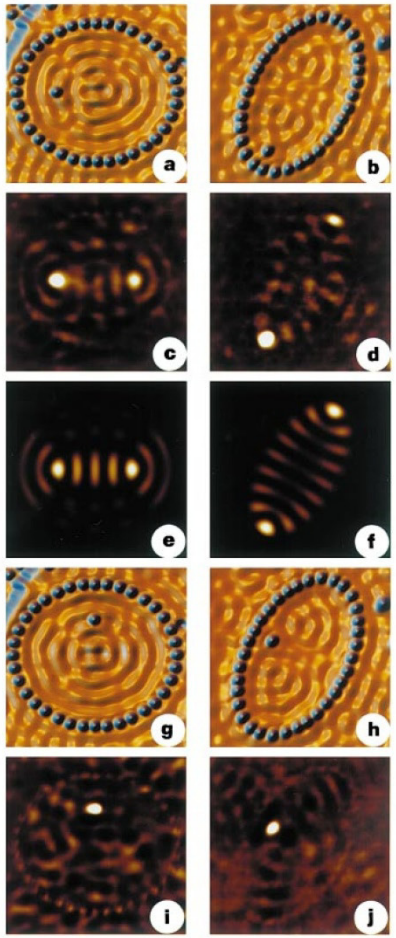

Figure 3 Visualization of the quantum mirage. **a**, **b**, Topographs showing the $e = 1/2$ (**a**) and $e = 0.786$ (**b**) ellipse each with a Co atom at the left focus. **c**, **d**, Associated d*I*/d*V* difference maps showing the Kondo effect projected to the empty right focus, resulting in a Co atom mirage. **e** and **f**, Calculated eigenmodes at E_F (magnitude of the wavefunction is plotted). When the interior Co atom is moved off focus (**g** and **h**, topographs), the mirage vanishes (**i** and **j**, corresponding d*I*/d*V* difference maps). Imaging conditions and dimensions as in Fig. 2. We have assembled over 20 elliptical resonators of varying size and eccentricity and searched for the formation of a quantum mirage. We find that as *a* is increased monotonically while *e* is fixed, the mirage is switched on and off. In each period of this switching, the classical path length $2a$ changes by a half Fermi wavelength. Because we also observe that two focal atoms, one on each focus, couple quite strongly with one another (as judged by the perturbation of the Kondo resonance) these oscillatory results may have a source akin to the RKKY (indirect exchange) interaction[19].

H. C. Manoharan, C. P. Lutz, D. M. Eigler, Quantum mirages formed by coherent projection of electronic structure, *Nature*, **403** (2000) 512.

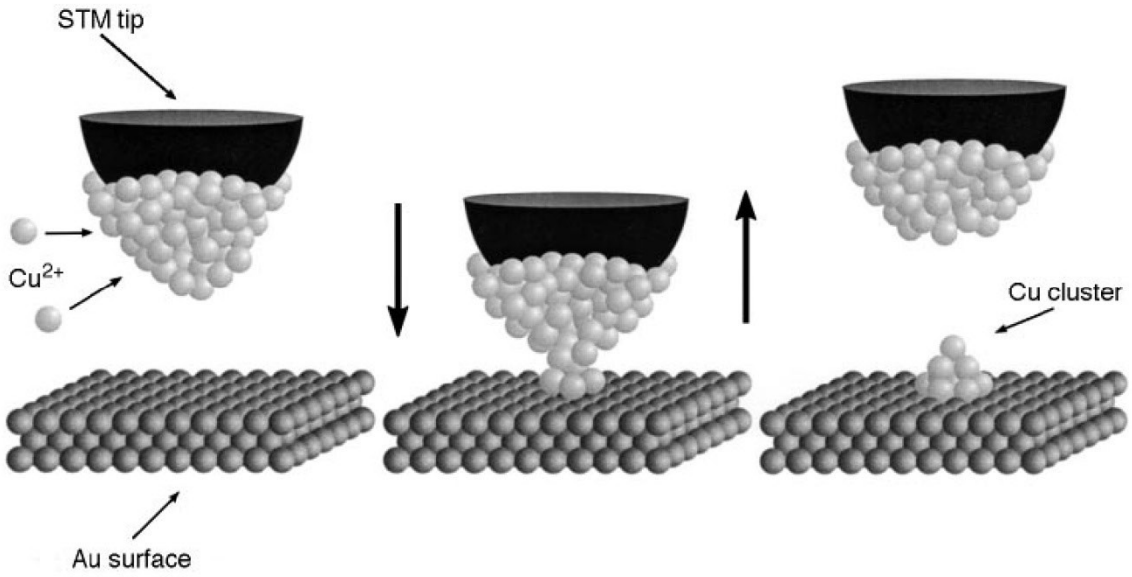

Fig. 2. Schematic diagram of the suggested mechanism of material transfer from a Cu-covered STM tip to the Au substrate, caused by an appropriate tip approach.

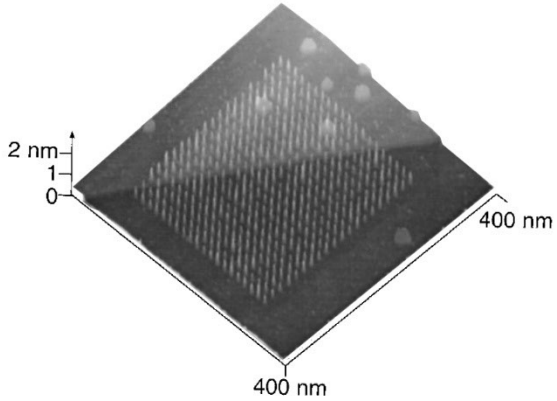

Fig. 4. STM image of an array of 400 Cu clusters on Au(111) in 0.05 M H_2SO_4 + 1 mM $CuSO_4$, covering an area 245 nm by 275 nm. E_{sample} = +10 mV; E_{tip} = −30 mV; I_T = 2 nA. The Cu clusters were generated by 400 single voltage pulses on the *z*-piezo while the tip was scanning over the surface. Tip approach Δz = 0.8 nm; pulse duration Δt = 2.5 ms.

D. M. Kolb, R. Ullmann, T. Will, Nanofabrication of Small Copper Clusters on Gold(111) Electrodes by a Scanning Tunneling Microscope, *Science* **275** (1997) 1097.

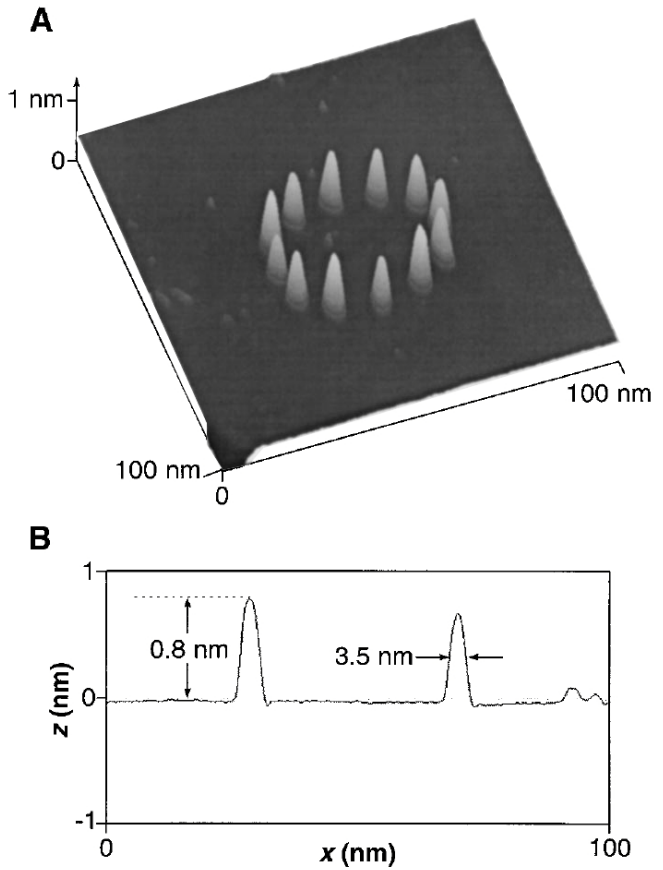

Fig. 3. (**A**) STM image of 12 Cu clusters on an Au(111) electrode in 0.05 M H_2SO_4 + 1 mM $CuSO_4$. E_{sample} = +10 mV; E_{tip} = −50 mV; I_T = 2 nA. The clusters were generated by 12 programmed approaches of the tip to the surface caused by external voltage pulses to the *z*-piezo. Tip displacement Δz = 1.6 nm; pulse duration Δt = 10 ms. (**B**) Cross section through the center of the circle (diameter, 41 nm), showing the height and FWHM of the Cu clusters.

D. M. Kolb, R. Ullmann, T. Will, Nanofabrication of Small Copper Clusters on Gold(111) Electrodes by a Scanning Tunneling Microscope, *Science* **275** (1997) 1097.

G.-Y. Liu, S. Xu, Y. Qian, Nanofabrication of Self-Assembled Monolayers Using Scanning Probe Lithography, *Acc. Chem. Res.* **33** (2000) 457-466

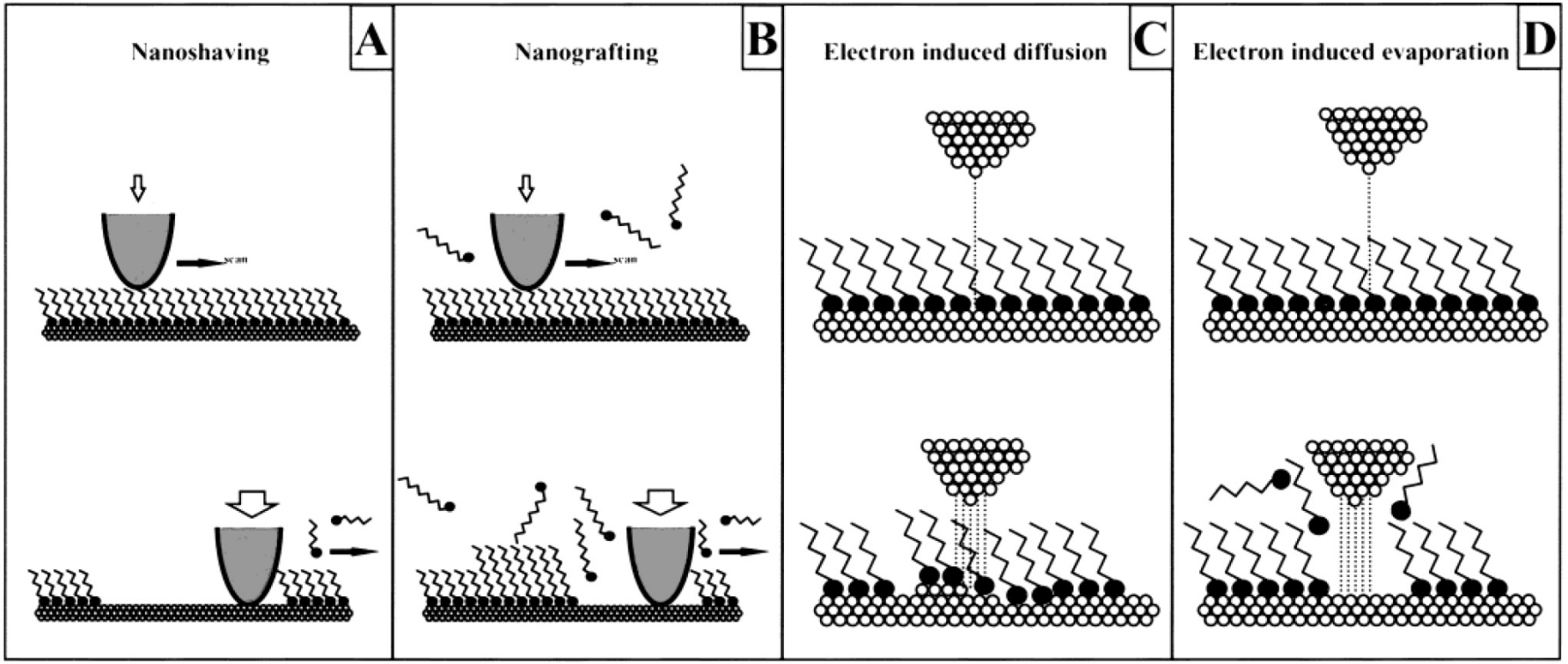

FIGURE 1. Schematic diagrams of four basic manipulation mechanisms using AFM (A and B) and STM (C and D). The imaging and fabrication modes are depicted in the top and bottom rows, respectively.

G.-Y. Liu, S. Xu, Y. Qian, Nanofabrication of Self-Assembled Monolayers Using Scanning Probe Lithography, *Acc. Chem. Res.* **33** (2000) 457-466

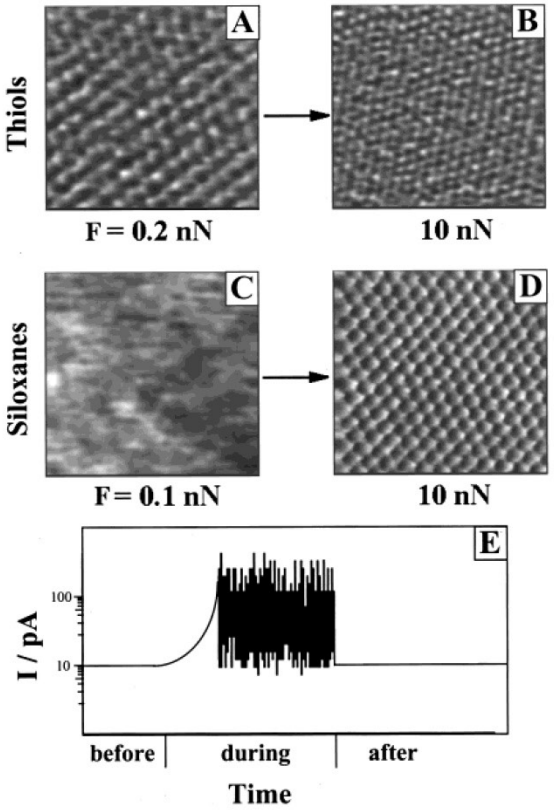

FIGURE 2. Determination of threshold force and tunneling current. Topographic images (5 × 5 nm²) of (A) $C_{18}S$/Au(111) and (C) OTE/mica taken in 2-butanol. At a load of 10 nN, images A and C changed into the periodicity of (B) Au(111) and (D) mica (0001), respectively. The threshold forces are 9.5 and 9.6 nN, respectively, which correspond to a pressure of 0.4 GPa based on the Hertzian model. (E) Sudden fluctuation occurs when the tunneling current causes diffusion or displacement.

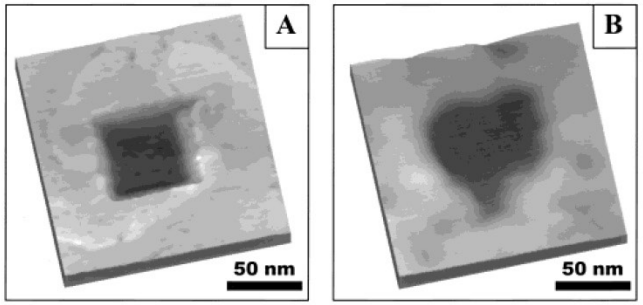

FIGURE 3. (A) 160 × 160 nm² topographic images of $C_{18}S$/Au(111) with the thiols shaved away from the central 50 × 50 nm² square. (B) 160 × 160 nm² topographic images of OTE/mica containing a heart-shaped pattern produced using nanoshaving.

G.-Y. Liu, S. Xu, Y. Qian, Nanofabrication of Self-Assembled Monolayers Using Scanning Probe Lithography, *Acc. Chem. Res.* **33** (2000) 457-466

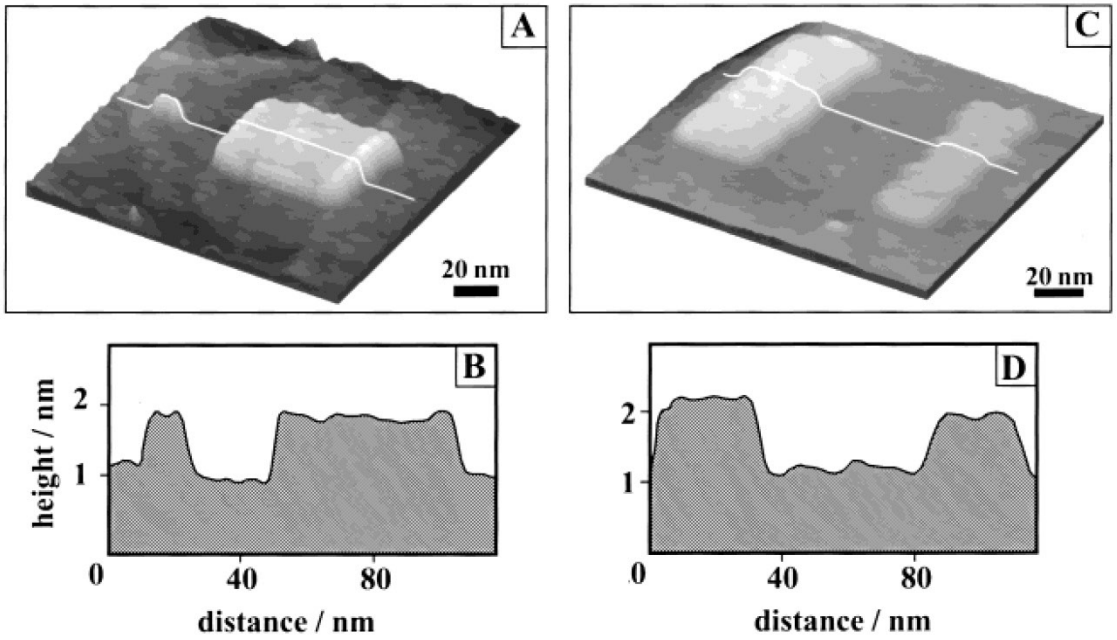

FIGURE 4. (A) Fabrication of two $C_{18}S$ nanoislands (3×5 and 50×50 nm^2) in the matrix of a $C_{10}S$ monolayer using nanografting. As shown in the cursor profile (B), the $C_{18}S$ islands are 8.8 Å higher than the surrounding $C_{10}S$ monolayer, consistent with the theoretical value for crystalline-phase SAMs. (C) Fabrication of multicomponent patterns using nanografting. The dimensions of the $C_{22}S$ (left) and $C_{18}S$ (right) islands are 30×60 and 20×60 nm^2, respectively. (D) The corresponding cursor profile shows that the $C_{18}S$ and $C_{22}S$ islands are 7.5 ± 1.0 and 12.0 ± 1.5 Å taller than the $C_{10}S$/Au matrix monolayer, respectively.

D. S. Ginger, H. Zhang, C. A. Mirkin, The Evolution of Dip-Pen Nanolithography, *Angew. Chem. Int. Edn.* **43** (2004) 30–45.

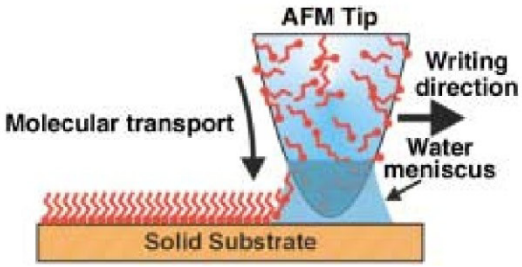

Figure 1. Schematic representation of the DPN process. A water meniscus forms between the AFM tip which is coated with "ink" molecules and the solid substrate. Reproduced with permission from ref. [1].

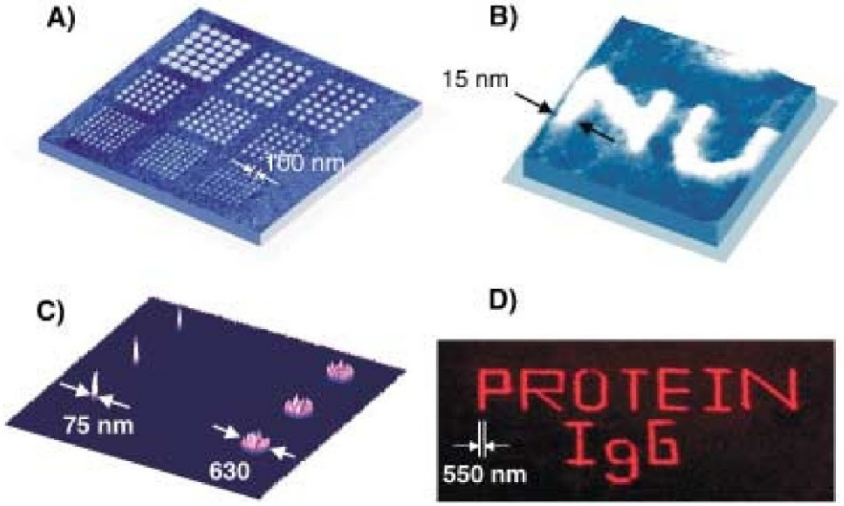

Figure 2. A) Nanoscale dot arrays written on a polycrystalline Au surface with mercaptohexadecanoic acid (MHA; thiohexadecanoic acid) by DPN[56] and B) nanoscale letters written on an Au(111) surface with MHA by DPN.[2] C) TM-AFM image of 25- and 13-nm gold nanoparticles hybridized to surface DNA templates generated with direct-write DPN (unpublished). D) Fluorescence image of direct-write DPN patterns of fluorescently labeled immunoglobulin G (IgG) on SiO_x.[46]

Scanning Probe Methods and Nanolithography

D. S. Ginger, H. Zhang, C. A. Mirkin, The Evolution of Dip-Pen Nanolithography, *Angew. Chem. Int. Edn.* **43** (2004) 30–45.

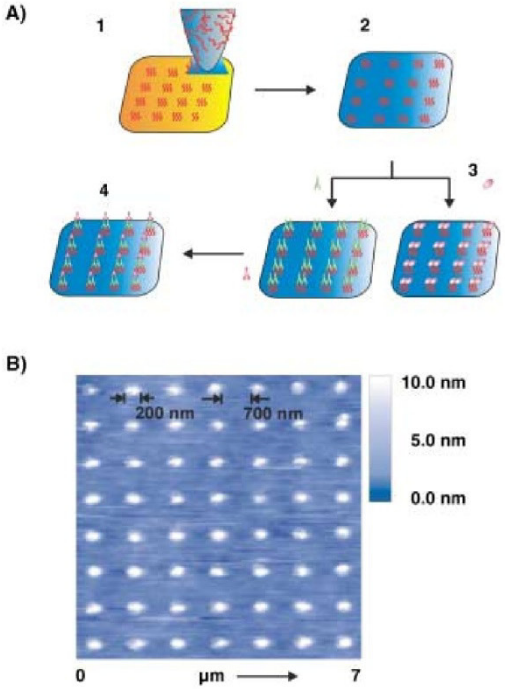

Figure 5. A) Diagram of proof-of-concept experiments, in which proteins were adsorbed on DPN-generated MHA patterns 1) MHA deposited from AFM tip onto surface, 2) passivation, 3) protein adsorption, 4) antibody recognition. The resulting protein arrays were then characterized by AFM. B) Topography image (contact mode AFM) of the retronectin protein array (reproduced with permission from ref. [34]).

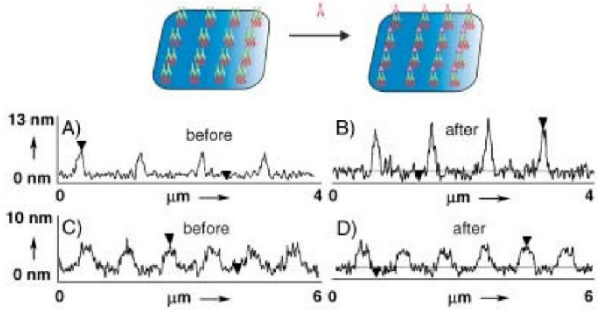

Figure 6. Height profiles of TM-AFM images: rabbit IgG assembled on an MHA dot array generated by DPN before (A) and after (B) treatment with a solution containing lysozyme, goat/sheep anti-IgG, human anti-IgG, and rabbit anti-IgG; a rabbit IgG nanoarray before (C) and after (D) exposure to a solution containing lysozyme, retronectin, goat/sheep anti-IgG, and human anti-IgG. (Portions reproduced with permission from ref. [34].)

Large-Area Nanoscale Patterning: Chemistry Meets Fabrication, J. Henzie, J. E. Barton, C. L. Stender, and T. W. Odom, *Acc. Chem. Res.* **39** (2006) 249-257.

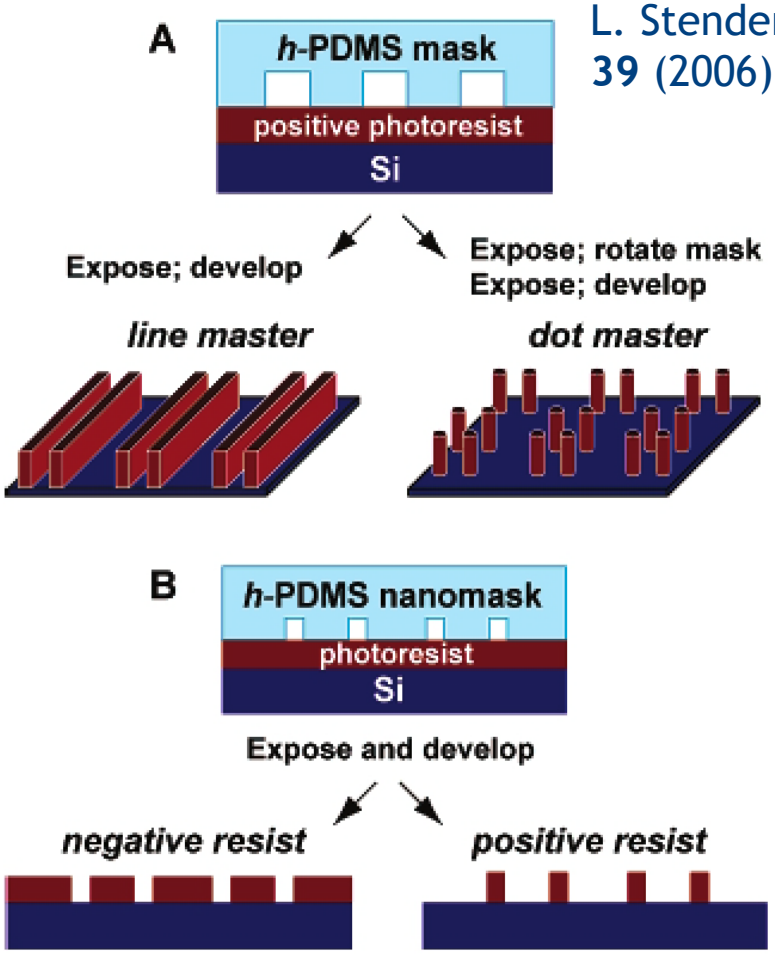

FIGURE 2. (A) Fabrication of nanoscale masters by PSP using *h*-PDMS masks patterned with microscale features and (B) sub-250 nm patterns in photoresist generated using *h*-PDMS nanomasks.

Large-Area Nanoscale Patterning: Chemistry Meets Fabrication, J. Henzie, J. E. Barton, C. L. Stender, and T. W. Odom, *Acc. Chem. Res.* **39** (2006) 249-257.

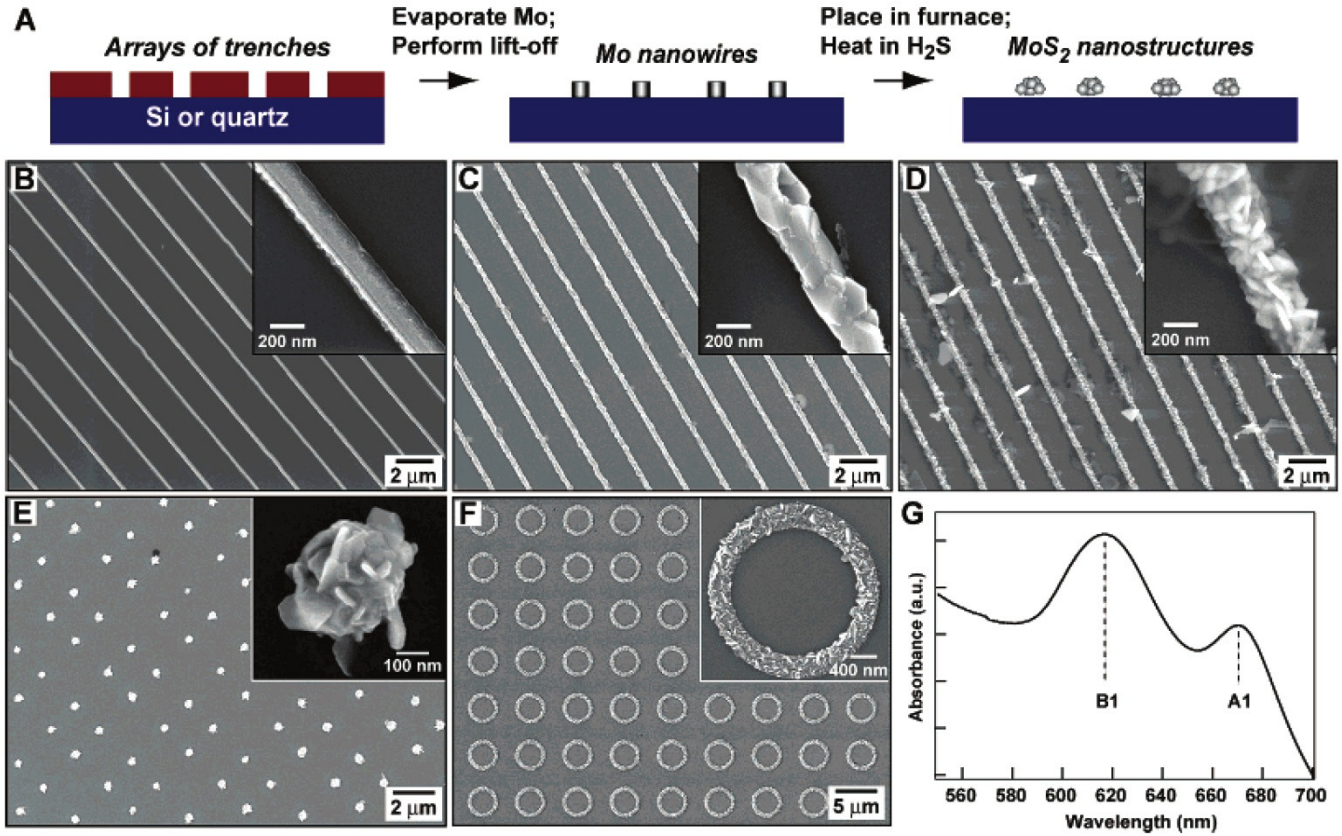

FIGURE 4. (A) Scheme for patterning MoS_2 nanostructures, (B) lines of Mo, (C) MoS_2 lines converted from panel B after reacting with H_2S gas, (D) MoS_2 lines converted from panel B with crystals oriented perpendicular to the surface, (E) MoS_2 dots, (F) rings of MoS_2 nanostructures, and (G) UV—visible absorption spectroscopy of a MoS_2 nanostructured film. Adapted from ref 19.